Available online at www.sciencedirect.com
SCIENCE DIRECT®
Journal of Nuclear Materials 340 (2005) 69–82
journal of nuclear materials
www.elsevier.com/locate/jnucmat

Thermodynamic considerations and prediction of the primary coolant activity of ^{99}Tc

B.J. Lewis [a,*], W.T. Thompson [a], F. Akbari [a], C. Morrison [a], A. Husain [b]

[a] Department of Chemistry and Chemical Engineering, Royal Military College of Canada, P.O. Box 17000, Kingston, Ont., Canada K7K 7B4

[b] Kinectrics Inc., 800 Kipling Avenue, Toronto, Ont., Canada M8Z 6C4

Received 6 April 2004; accepted 13 October 2004

Abstract

A physical model has been developed to describe the coolant activity behaviour of ^{99}Tc, during constant and reactor shutdown operations. This analysis accounts for the fission production of technetium and molybdenum, in which their chemical form and volatility is determined by a thermodynamic treatment using Gibbs-energy minimization. The release kinetics are calculated according to the rate-controlling step of diffusional transport in the fuel matrix and vaporization from the fuel-grain surface. Based on several in-reactor tests with defective fuel elements, and as supported by the thermodynamic analysis, the model accounts for the washout of molybdenum from the defective fuel on reactor shutdown. The model also considers the recoil release of both ^{99}Mo and ^{99}Tc from uranium contamination, as well as a corrosion source due to activation of ^{98}Mo. The model has provided an estimate of the activity ratio ^{99}Tc/^{137}Cs in the ion-exchange columns of the Darlington Nuclear Generating Station, i.e., 6×10^{-6} (following ~200 days of steady reactor operation) and 4×10^{-6} (with reactor shutdown). These results are consistent with that measured by the Battelle Pacific Northwest Laboratories with a mixed-bed resin-sampling device installed in a number of Pressurized Water Reactor and Boiling Water Reactor plants.

1. Introduction

Radionuclides such as ^{14}C, ^{94}Nb, ^{3}H, ^{36}Cl, ^{59}Ni, ^{99}Tc, ^{129}I, ^{79}Se, and the actinide isotopes of U, Th, Pu, Pa, Am and Np, are of potential interest to the long-term management of low and intermediate level wastes. Most of these radionuclides are difficult-to-measure (DTM) because they are non-gamma emitting and consequently scaling factors are required to estimate their concentrations for reactor waste management. Scaling factors for several radionuclides of interest can be estimated from their activities in the reactor coolant system. Due to the much lower concentrations of many of the DTM radionuclides, e.g., ^{129}I and ^{99}Tc, their experimental scaling factor development poses a major challenge and theoretical treatments have been proposed for their estimation [1–3]. The PROFIP code, for instance, has been developed to estimate coolant activity concentrations of fission products and actinides in pressurized water reactors (PWRs) [1]. Similarly, the 3R-STAT code

* Corresponding author. Tel.: +1 613 5416611; fax: +1 613 5429489.
E-mail address: lewis-b@rmc.ca (B.J. Lewis).

0022-3115/$ - see front matter
doi:10.1016/j.jnucmat.2004.10.116

focuses on an estimation of ^{129}I and ^{99}Tc coolant activities using measured activities of ^{60}Co, ^{137}Cs and short-lived radioiodine species [3].

For CANDU reactor analysis, a method has been recently proposed for predicting the coolant activity of the long-lived ^{129}I, and its scaling factor relative to that of ^{137}Cs, based on the measured coolant activities of the short-lived iodine species [4]. In this paper, the model is extended for estimation of the coolant activity of the long-lived ^{99}Tc (half-life of 2.13×10^5 years). This work involves the computed isothermal phase equilibrium of Mo and Tc in liquid water as portrayed in Pourbaix diagrams, and the volatility of these species in a steam atmosphere with a Gibbs energy minimization procedure [5–7]. Based on insights provided by the thermodynamic analysis, a fission product release model is developed considering the physical mechanisms of release from defective fuel elements and uranium contamination on in-core surfaces [8–16].

2. Model development

With defective fuel, there is a breach in the cladding so that primary coolant can enter into the fuel element and fission products can escape through the defect site into the heat-transport system. A thermodynamic analysis is used to describe the leaching behaviour of fission products (i.e., Mo and the daughter product Tc) during reactor shutdown conditions (Section 2.1), and their release behaviour with a steam environment present in the gap during steady reactor operation (Section 2.2). Finally, based on the thermodynamic predictions, and from in-reactor experiments at the Chalk River Laboratories (CRL), a mathematical treatment is developed from mass balance considerations to predict the time-dependent coolant activity behaviour of ^{99}Tc during constant power operation and for reactor shutdown situations (Section 2.3). This model considers the possibility of fission product release of ^{99}Mo and ^{99}Tc from both defective fuel and uranium contamination on in-core surfaces. A possible source of ^{99}Tc resulting from the corrosion and activation of ^{98}Mo is also considered.

2.1. Thermodynamic analysis for reactor shutdown conditions

During reactor shutdown, the primary coolant is in the liquid state in the fuel-to-clad gap of a defective element and is therefore in direct contact with the uranium dioxide fuel and any fission products exposed to the free surfaces. The redox potential, E_h, and pH are important variables in understanding the isothermal phase equilibrium of a particular element in liquid water, i.e., the phase equilibrium can be represented in a E_h-pH space with Pourbaix diagrams [5,6]. These diagrams can in fact be developed more generally with a Gibbs energy minimization procedure, using the Facility for the Analysis of Chemical Thermodynamics (FACT) [7]. This latter approach is capable of considering all of the candidate chemical species of a particular element (e.g., U) potentially dissolved (e.g., $UO_2^{2+}, \ldots$) or in contact with water (e.g., $U_4O_9, \ldots$).

For instance, consider the formation of all possible U–H–O species from a mole of U in its most stable allotropic form (orthorhombic) at a given temperature using a minimization procedure. The formation reactions are balanced using only H_2O, H^+ and e^-. These reactions are listed in Table 1 with the standard Gibbs energy changes (i.e., at E_h (S.H.E.) = 0, pH = 0 and molality m (activity) = 1) for 298 and 523 K. To build a Pourbaix diagram over the desired range of E_h and pH, adjustments are made to the standard Gibbs energies in Table 1 to reflect departure from the standard state condition. The steps in the incremental changes of E_h and pH are conveniently made the same. At each step, the Gibbs energies in Table 1 are adjusted by the following change in Gibbs energy:

$$\Delta G_{H^+} = -2.303RT \text{ pH}, \tag{1}$$

$$\Delta G_{e^-} = -\Im E_h, \tag{2}$$

where $\Im$ is the Faraday constant, R is the ideal gas constant and T is the absolute temperature. For the treatment of the 'electron', the symbol 'e^-' represents an unspecified process in the water phase that controls the redox potential, e.g., dissolved oxygen:

$$1/2\,O_2 + 2H^+ + 2e^- = H_2O. \tag{3}$$

When Eq. (2) is used, one is in effect finding the Gibbs energy change for a process such as Eq. (3) for some particular dissolved oxygen concentration and pH, which determines E_h at that temperature. Pourbaix diagrams generally show the influence of concentration of aqueous species, which has the effect of enlarging the aqueous domains as dilution increases. This aspect of diagram development involves adjusting the Gibbs energies in Table 1 (per mole of U-containing ion) by ($RT\ln m$) (very nearly the thermodynamic activity in dilute solutions). With all Gibbs energies in Table 1 adjusted for concentration, E_h and pH, the lowest value is then found. This identifies the particular U-containing species that is most stable. By repetition of this process for each E_h-pH point on the diagram, the domains of the different species can be established.

2.1.1. Pourbaix diagrams for Uranium

The Uranium Pourbaix diagram at 298 K covering the range of redox potential pertinent to fuel oxidation is shown in Fig. 1. The data for UO_2, U_4O_9, U_3O_7 and U_3O_8 is the same as that used for the U–O binary phase diagram [17]. Placed on the diagram for reference are dashed lines ⓐ and ⓑ corresponding to redox potentials

Table 1
Formation of Uranium compounds and associated changes in standard Gibbs energy (ΔG^o) (J/mol)

Reaction	$T = 298$ K	$T = 523$ K
$U_{(S1)}$[a] → $U_{(S1)}$	0.00	0.00
$U_{(S1)} \rightarrow U_{(S2)}$[b]	1899.90	1241.30
$U_{(S1)} \rightarrow U_{(S3)}$[c]	3914.00	3482.00
$U_{(S1)} \rightarrow U_{(l)}$	6172.10	6184.20
$U_{(S1)} \rightarrow U_{(g)}$	453 513.40	427 471.30
$U_{(S1)} \rightarrow U^{3+}_{(aq)} + 3e^-$	−520 616.30	−519 115.40
$U_{(S1)} \rightarrow U^{4+}_{(aq)} + 4e^-$	−531 821.30	−200 331.40
$U_{(S1)} + 3H^+ + 3e^- \rightarrow UH_{3(S)}$	−72 773.10	−30 178.60
$U_{(S1)} + H_2O_{(l)} \rightarrow UO_{(g)} + 2H^+ + 2e^-$	252 146.10	196 803.90
$U_{(S1)} + 2H_2O_{(l)} \rightarrow UO_{2(S)} + 4H^+ + 4e^-$	−557 615.50	**−587 272.20**
$U_{(S1)} + 2H_2O_{(l)} \rightarrow UO_{2(g)} + 4H^+ + 4e^-$	3336.20	−68 516.70
$U_{(S1)} + 2H_2O_{(l)} \rightarrow UO^+_{2(aq)} + 4H^+ + 5e^-$	−519 894.80	−557 462.90
$U_{(S1)} + 2H_2O_{(l)} \rightarrow UO^{2+}_{2(aq)} + 4H^+ + 6e^-$	−514 898.70	−537 165.70
$U_{(S1)} + 3H_2O_{(l)} \rightarrow UO_{3(g)} + 6H^+ + 6e^-$	−70 484.60	−162 354.80
$U_{(S1)} + H_2O_{(l)} \rightarrow UOH_{(g)} + H^+ + e^-$	307 110.70	260 552.80
$U_{(S1)} + H_2O_{(l)} \rightarrow UOH^{3+}_{(aq)} + H^+ + 4e^-$	**−572 299.70**	−565 411.70
$U_{(S1)} + 2H_2O_{(l)} \rightarrow UO_2H_{2(g)} + 2H^+ + 2e^-$	145 653.40	87 541.20
$U_{(S1)} + 2H_2O_{(l)} \rightarrow H_2O_2U^{2+}_{(aq)} + 2H^+ + 4e^-$	−516 616.60	−508 411.80
$U_{(S1)} + 3H_2O_{(l)} \rightarrow HO_3U^+_{(aq)} + 5H^+ + 6e^-$	−445 431.20	−471 213.50
$U_{(S1)} + 3H_2O_{(l)} \rightarrow H_3O_3U^+_{(aq)} + 3H^+ + 4e^-$	−499 464.10	−495 250.50
$U_{(S1)} + 4H_2O_{(l)} \rightarrow UO_3(H_2O)_{(S)} + 6H^+ + 6e^-$	−452 724.20	−488 621.70
$U_{(S1)} + 4H_2O_{(l)} \rightarrow UO_3(H_2O)_{(g)} + 6H^+ + 6e^-$	121 398.80	−272 630.90
$U_{(S1)} + 5H_2O_{(l)} \rightarrow UO_3(H_2O)_{2(S)} + 6H^+ + 6e^-$	−450 988.20	−482 405.00
$U_{(S1)} + 5H_2O_{(l)} \rightarrow U(OH)^-_{5(aq)} + 5H^+ + 4e^-$	−444 786.40	−393 496.50
$U_{(S1)} + 3H_2O_{(l)} \rightarrow 1/2H_2O_6U^{2+}_{2(aq)} + 5H^+ + 6e^-$	−462 436.05	−476 622.80
$U_{(S1)} + 11/3H_2O_{(l)} \rightarrow 1/3H_5O_{11}U_{3(aq)}{}^+ + 17/3H^+ + 18/3e^-$	−448 733.13	−461 034.10
$U_{(S1)} + 13/3H_2O_{(l)} \rightarrow 1/3(UO_2)_3(OH)^-_{7(aq)} + 19/3H^+ + 18/3e^-$	−419 888.60	−451 324.63
$U_{(S1)} + 3H_2O_{(l)} \rightarrow UO_{3(S)} + 6H^+ + 6e^-$	−434 199.50	−484 106.00
$U_{(S1)} + 7/3H_2O_{(l)} \rightarrow 1/3U_3O_{7(S)} + 14/3H^+ + 14/3e^-$	−526 604.97	−566 387.10
$U_{(S1)} + 8/3H_2O_{(l)} \rightarrow U_3O_{8(S)} + 16/3H^+ + 16/3e^-$	−490 250.80	−534 872.97
$U_{(S1)} + 9/4H_2O_{(l)} \rightarrow 1/4U_4O_{9(S)} + 18/4H^+ + 18/4e^-$	−535 375.90	−573 954.03

[a] $U_{(S1)}$ = orthorhombic (298–942 K).
[b] $U_{(S2)}$ = tetragonal (942–1049 K).
[c] $U_{(S3)}$ = cubic (1049–1405 K).

associated with hydrogen and oxygen saturation (i.e., at 1 atm), respectively. The origin of Fig. 1(b) provides a simple check of the foregoing Gibbs energy minimization, since there is no need to make any Gibbs energy adjustment to Table 1. The species UOH^{3+} with the lowest Gibbs energy of formation is indeed dominant on the Pourbaix diagram at $E_h = 0$ and pH = 0.

Since the Gibbs energy changes for the reactions in Table 1 vary linearly with E_h and pH, each species in Table 1 can be associated with a plane in ΔG–E_h-pH space. The envelope of lowest planes viewed normal to the E_h-pH plane provides the Pourbaix diagram for the fixed concentration that applies to each aqueous species. This result is illustrated in Fig. 2, which can be related to the domains on the Pourbaix diagram in Fig. 1 at 10^{-6} molal. The effect of raising the temperature to 523 K for the uranium Pourbaix diagram is shown in Fig. 3.

2.1.2. Pourbaix diagrams for Molybdenum and Technetium

In the case of Mo, the data yielding the diagrams in Fig. 4(a) (i.e., 298 K) and (b) (i.e., 523 K) are shown in

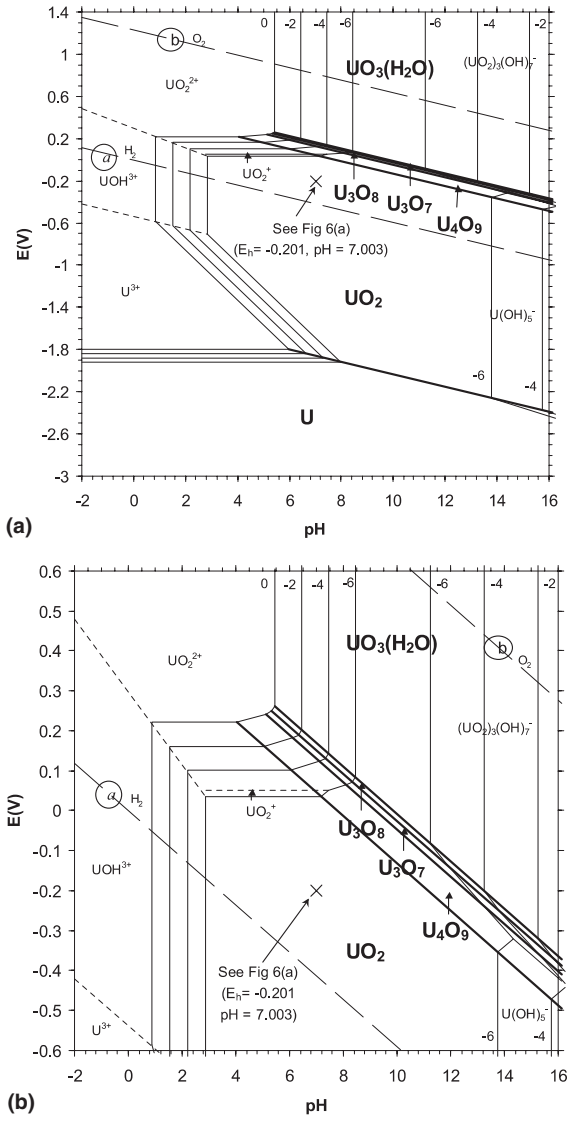

Fig. 1. (a) U–H_2O Pourbaix diagram calculated with FACT at 298 K, and (b) enlargement of the region in (a) bounded by the dashed lines ⓐ and ⓑ which represent hydrogen and oxygen saturation at 1 atm partial pressure.

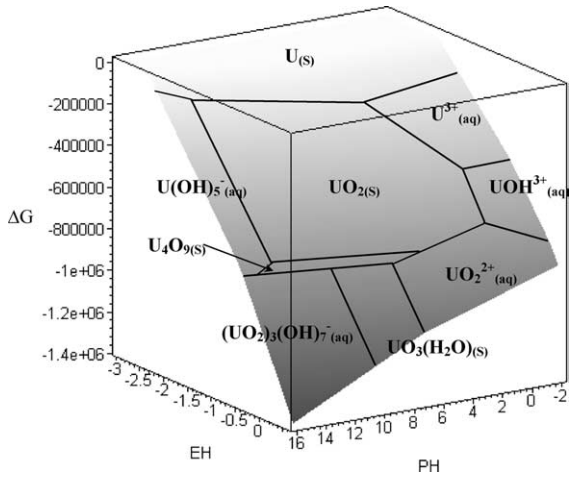

Fig. 2. The minimum surface of values for changes in Gibbs Energy for all U–OH compounds in an aqueous system at 298 K; concentration of aqueous species is 10^{-6} molal. The figure has been simplified in the area near U_4O_9.

Table 2 [7]. The diagrams for Tc in Fig. 5(a) and (b) are similarly developed from the Gibbs energies in Table 3. The Gibbs energy changes for TcO_2 and TcO_4^- incorporate the data of Lemire and Jobe [18]. Under strongly acid conditions, it appears that $HTcO_4$ can develop. The dissociation constant for:

$$HTcO_{4(aq)} = TcO^-_{4(aq)} + H^+_{(aq)} \quad (4)$$

is believed to be near unity so the properties for $HTcO_4$ were adjusted to be consistent with Lemire and Jobe [18]. The greater stability of TcO_2 [18] has the effect of eliminating TcO_3 as a stable phase from the diagram. Also note, as a point of connection with Table 3, that the Tc metal field covers the area near $E_h = 0$ and pH = 0 since the standard Gibbs energies of all other Tc species are positive.

The Pourbaix diagrams can now be used to determine the leaching of Mo and/or Tc fission products from UO_2 fuel. The radioisotope ^{99}Mo can decay radioactively into the isomeric state ^{99m}Tc and the ground state ^{99}Tc as discussed in Section 2.3 during reactor operation and following reactor shutdown. Mo and Tc are principally found in association with Ru, Rh and Pd in metallic inclusions in partially burned or spent fuel [19,20]. Since UO_2 is by far the dominant solid phase, the redox potential of the water will eventually be controlled by the UO_2 water reactions (e.g., Fig. 1). Fig. 6(a) shows the most stable species from among all of those associated with Table 1 when 1 mol of UO_2 reaches an equilibrium in 1 kg (55.5 mol) of H_2O at 298 K. The computation, based on Gibbs energy minimization [21,22] with data in Table 1, is truncated at concentrations (activities) of 10^{-10} m. This result is in keeping with Fig. 1. The computed redox potential (−0.201 V (SHE)) and pH (7.003) in Fig. 6(a) locates a point in the field of UO_2 on Fig. 1, where the concentration of the most populous U-containing ion, UO_2^+ is well below 10^{-6} molal. Fig. 6(b) repeats the calculations for 523 K with the pressure raised to suppress boiling. In particular, this temperature (i.e., 523 K) and pressure (i.e., 100 atm) is relevant to the coolant conditions in the primary heat transport system of the CANDU reactor.

The disposition of Mo and Tc can now be understood, in principle, using the equilibrium thermodynam-

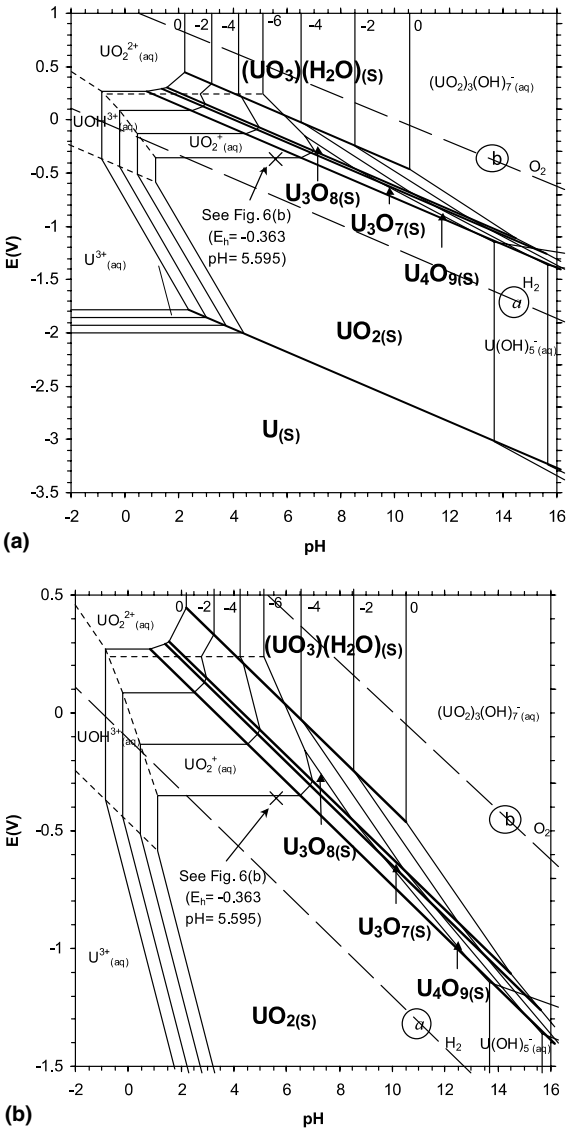

Fig. 3. FACT generated U–H_2O Pourbaix diagram for 523 K, and (b) enlargement of the region in (a) bounded by the dashed lines ⓐ and ⓑ which represent hydrogen and oxygen saturation at 1 atm partial pressure.

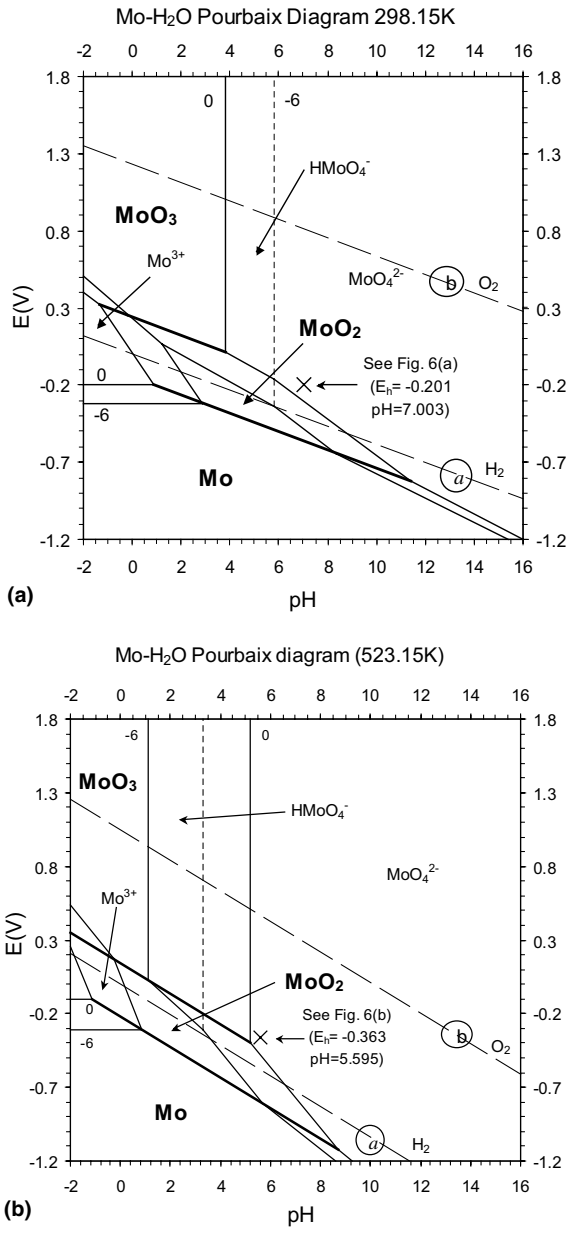

Fig. 4. FACT generated Mo-H_2O Pourbaix diagram for (a) 298 K and (b) 523 K.

ics depicted on the Pourbaix diagrams in Figs. 4 and 5 since the appropriate E_h and pH have been determined. Mo is oxidized principally to MoO_4^{2-} ions. Because of the proximity to the $HMoO_4^-$ domain, this species would be the next most populous ion. The distance from the Mo^{3+} domain indicates that the concentration of this ion would likely be below detection. The solid oxide MoO_3 is very unstable. The oxide MoO_2 might be found as an unstable intermediate during the course of Mo (metal) becoming MoO_4^{2-}. In the case of Tc, the redox potential and pH associated with Fig. 6, places a point on or near the Tc/TcO_2 phase boundary. With the Lemire and Jobe data for TcO_2, [18] this is the more stable phase. With other data, [7] Tc remains unoxidized. In any event, conditions are far away from detectable concentrations of aqueous species TcO_4^-, $HTcO_4$ or Tc^{2+}. Hence, all of this implies that if Tc were detected in the water phase, it could only arise (in the absence of dissolved oxygen) as a result of the decay of Mo (which the Pourbaix diagram in Fig. 4 indicates can be easily leached).

Table 2
Gibbs energy changes for Mo species (kJ/mol)

Reaction	298 K	523 K
$Mo_{(S)} = Mo_{(S)}$	0.00	0.00
$Mo_{(S)} = Mo^{3+}_{(aq)} + 3e^-$	**−57.86**	−29.91
$Mo_{(S)} + 2H_2O = MoO_{2(S)} + 4H^+ + 4e^-$	−57.63	**−84.91**
$Mo_{(S)} + 3H_2O = MoO_{3(S)} + 6H^+ + 6e^-$	−11.34	−57.38
$Mo_{(S)} + 4H_2O = MoO^{2-}_{4(aq)} + 8H^+ + 6e^-$	43.50	46.83
$Mo_{(S)} + 4H_2O = HMoO^-_{4(aq)} + 7H^+ + 6e^-$	10.42	13.75

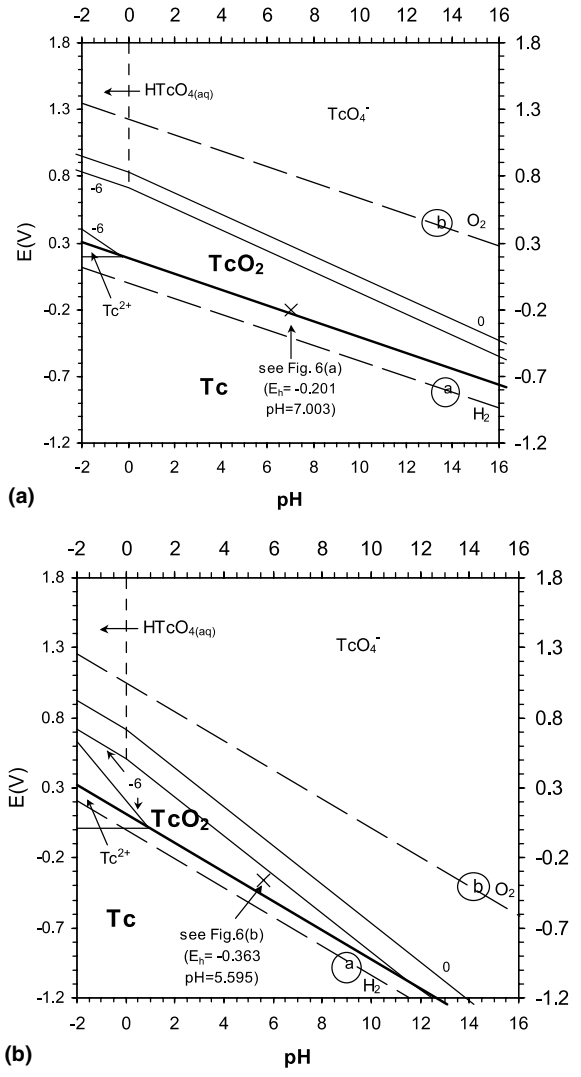

Fig. 5. FACT generated Tc-H_2O Pourbaix diagram for (a) 298 K and (b) 523 K.

2.2. Thermodynamic analysis for steady reactor operation

A thermodynamic analysis, based on a Gibbs-energy minimization, was further carried out with FACT in order to determine the speciation of the Mo and Tc fission products in a steam environment [7]. This analysis was performed on the basis of a Bruce fuel channel. In particular, the analysis considered the fission product inventory in the fuel bundles of the channel (i.e., as estimated with the ORIGEN code at a fuel burnup of 100 MWh/kgU),[23] and the relative volumes of the fuel bundles to free space in the channel for the atmospheric constituent. This approach essentially assumes an unlimited supply of steam and water into the fuel-to-clad gap where there is an open system with the possibility of a continual replenishment of steam/water from the primary coolant into the failed rod. A sample calculation can be seen in Fig. 7.

Fig. 8 shows the predicted partial pressures p_{Tc} and p_{Mo} for the elements of Tc and Mo. Due to the higher volatility for Mo, the release from the fuel matrix to the fuel-to-clad gap will be dominated solely by this precursor product. The dominant gaseous compound for this species is MoOH over possible fuel temperatures for defective fuel in the presence of steam (i.e., ranging from a typical fuel surface temperature of ~400 °C up to near the melting temperature of ~2800 °C for the hyperstoichiometric fuel) and system pressure (100 atm). However, the Mo partial pressure is significantly reduced at the cooler fuel surface where it will be present as a condensed solid phase (i.e., MoO_2 and Cs_2MoO_4).

2.3. Fission product release model

As shown in Section 2.1.2, the Tc will not be released from the water-filled gap on shutdown. On the other hand, Mo is readily soluble under aqueous conditions so that it will be rapidly washed out of the defective rod as MoO^{2-}_4. In fact, these predictions are consistent with observations from experimental loop irradiations at the CRL with defective fuel rods [15,24]. In addition, in agreement with Section 2.2, leaching experiments were performed on spent CANDU rods to measure the combined gap and grain-boundary inventories of ^{137}Cs, ^{129}I, ^{90}Sr, ^{99}Tc and ^{14}C, which suggested that technetium is not a volatile species and was unlikely to be found in the gap [25]. It was further suggested that the diffusion coefficient for Tc is considerably smaller than that of Xe, Cs or I [25,26], Data on diffusion coefficients for Tc during normal reactor operating conditions are scarce. However, Prussin et al. also suggest lower diffusion coefficients for Tc compared to that of Xe, I and Cs although these data are for trace-irradiated fuel [27]. In agreement with the FACT thermodynamic analysis in Section 2.2, [20] it is further noted that Tc will be found as metallic precipitates (with Mo, Ru, Rh and Pd) on the grain boundaries and as metallic alloy inclusions [28–30].

Hence, as indicated from the thermodynamic calculations (where it is indicated that Mo is present as a con-

Table 3
Gibbs energy changes for Tc species (kJ/mol)

Reaction	298 K	523 K
$Tc_{(S)} = Tc_{(S)}$	**0.00**	**0.00**
$Tc_{(S)} = Tc^{2+}_{(aq)} + 2e^-$	71.93	63.53
$Tc_{(S)} + 2H_2O = TcO_{2(S)} + 4H^+ + 4e^-$	69.58	67.28 [18]
$Tc_{(S)} + 3H_2O = TcO_{3(S)} + 6H^+ + 6e^-$	252.35	208.19
$Tc_{(S)} + 4H_2O = TcO^-_{4(aq)} + 8H^+ + 7e^-$	311.4	250.73 [18]
$Tc_{(S)} + 4H_2O = HTcO_{4(aq)} + 7H^+ + 7e^-$	311.4	250.73 [18]

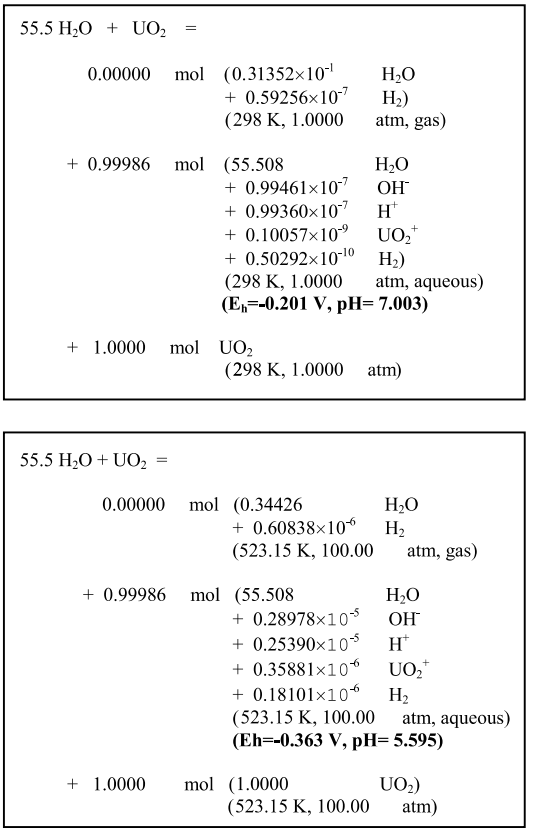

Fig. 6. Gibbs Energy Minimization of UO_2 in one kg of H_2O for (a) 298 K and (b) 523 K for purposes of determining the redox potential. A pressure of 100.0 atm is considered in (b) to maintain an aqueous phase.

densed but water-soluble phase at the fuel surface), and as specifically observed from in-reactor experiments with defective fuel elements at the Chalk River Laboratories, it is assumed that Mo is released from the defective fuel rod as a result of washout during reactor shutdown/startup but it is not released under dry steam conditions during steady reactor operation for the fission product release model. The gap inventory develops from: (i) solid-state diffusion through the solid matrix, and (ii) vaporization from the fuel grain surface with gas-phase transport through the tunnel interlinkage. The release kinetics are therefore controlled by the rate-limiting step between these two processes. The Mo that eventually reaches the gap will be stored there (i.e., as a condensed phase) until the occurrence of a transient event. Technetium that is produced in the gap by the decay of Mo is not mobile. This treatment is also in agreement with that proposed by Vance for the 3R-STAT model, where no Tc source release is assumed to occur from the defective rod itself [3]. On the other hand, both Mo and Tc may be directly released by a recoil fission process from uranium contamination that is deposited on in-core piping surfaces.

2.3.1. Fission product release rate from the fuel matrix

For the relatively short-lived ^{99}Mo (half-life of 66.02 h), an equilibrium situation is quickly reached so that the release rate for diffusion R_{dif} (atom s^{-1}) from the fuel matrix to the fuel-to-clad gap is given by the steady-state relation: [4]

$$R_{dif} = 3\left[\frac{1}{\sqrt{\mu}}\coth\sqrt{\mu} - \frac{1}{\mu}\right]Fy \approx 3\sqrt{\frac{D'}{\lambda}}Fy, \tag{5}$$

where $\mu = \lambda/D'$, λ is the decay constant, F is the fission rate (fission s^{-1}) and y is the cumulative fission yield for ^{99}Mo. The empirical diffusion coefficient D' (s^{-1}) in the fuel matrix can be obtained from a correlation developed from in-reactor loop experiments with defective CANDU fuel rods operating at a linear power P (kW/m): [14]

$$D'_{\text{Iodine}} = 10^{9.857\log P - 25.1314}. \tag{6}$$

This result can be used since it has been shown in high-temperature annealing experiments that I, Cs, Kr, Xe and Mo have similar diffusivities [23,31].

The release rate for vaporization R_{vap} (atom s^{-1}) can be derived from a mass-transfer model based on the Fick's law of diffusion:

$$R_{vap} = \gamma S_{eff} N_A k_{im}(\bar{x}^{gs} - x^g), \tag{7}$$

where γ (=1) is the number of atoms per molecule of the dominant volatile compound for Mo (i.e., MoOH), S_{eff} is the effective grain-boundary surface area exposed to the gap (m^2), $\bar{x}^{gs}$ is the average mole fraction of the Mo-bearing gaseous compound at the grain surface, x^g is the mole fraction in the gap (~0) and N_A is Avogadro's number. The mass transfer coefficient k_{im} (mol m^{-2} s^{-1}) is defined as

$$k_{im} = \frac{cD_{AB}}{\ell}, \tag{8}$$

where the quantity cD_{AB} can be evaluated from Chapman-Enskog kinetic theory for Mo diffusing in a continuum steam medium at an average fuel temperature T

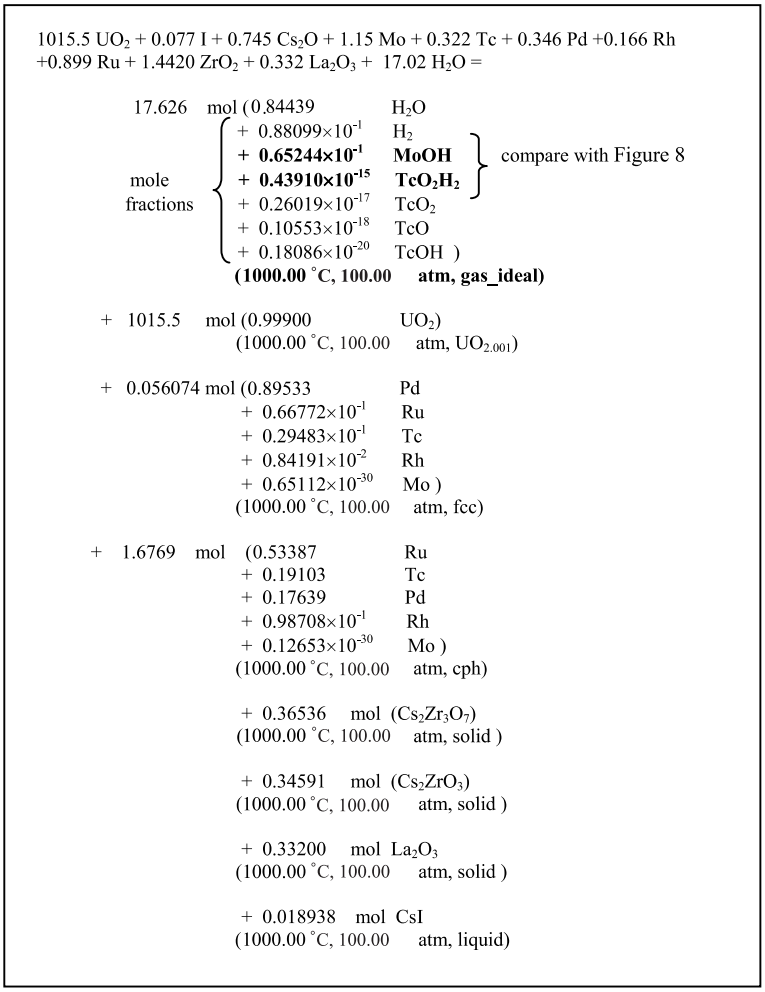

Fig. 7. Sample calculation regarding steady state reactor operation in steam at 1000 °C. Notice that partial pressure of Mo in gas phase is ($0.65244 \times 10^{-1} \times 100$ atm.) and for Tc is ($0.43910 \times 10^{-15} \times 100$ atm). The other Tc-containing species contributions to increase the partial pressure of Tc in gas phase are insignificant.

[23,32] and ℓ is a characteristic transport-path length through the tunnel interlinkage to the gap (m) (which is approximately equal to the pellet radius). The mole fraction $\bar{x}^{gs}_{Mo} = \bar{p}_{Mo}/p_T$ can be estimated by averaging the Mo partial pressures in Fig. 8 over the fuel pellet volume using a given temperature profile for the defective fuel element for a given system pressure $p_T = 100$ atm [33].

2.3.2. ^{99}Tc coolant activity prediction

The overall release rate of Mo from the fuel matrix into the gap is therefore taken as the rate-determining step between solid-state diffusion to the fuel grain surface (R_{dif}) and vaporization from the grain surface (R_{vap}). For a defective element operating under normal conditions at low (25 kW/m) and high power (52 kW/m), Eqs. (5) and (7) indicate that diffusion is the rate-limiting step for Mo release into the gap. Hence, ^{99}Mo will diffuse into the fuel-to-clad gap via Eq. (5), where it is stored during the steady operating period. Consequently, from the mass balance, the steady-state activity in the gap is $A_{go} = R_{dif}$. On a subsequent reactor shutdown, this stored activity is quickly released into the primary heat transport system (PHTS) as an instantaneous process, according to [4]

$$A_c(t) = [A_{co} + A_{go}]e^{-(\lambda+\beta_{S/D})t}, \tag{9}$$

where $A_c(t)$ is the coolant activity of ^{99}Mo at time t following a shutdown, $\beta_{S/D}$ is the purification constant during shutdown and A_{co} is the initial coolant activity at the time of shutdown. This latter contribution is developed

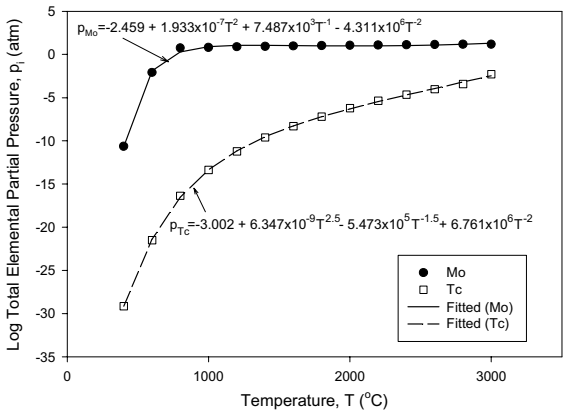

Fig. 8. Variation of partial pressure of the total amount of the elements of Mo and Tc with temperature T (in °C). Compare the partial pressure at 1000 °C with typical calculations shown in Fig. 7.

during the previous steady operating period from the tramp uranium contamination (Section 2.3.2.1) or through activation of the corrosion product, ^{98}Mo (Section 2.3.2.2). Thus, Eq. (9) yields a source release of ^{99}Mo into the coolant which will decay into the daughter product, ^{99}Tc (Section 2.3.2.3).

2.3.2.1. Tramp Uranium release. Uranium contamination resulting from a previous fuel loss from defective fuel rods or from the fuel manufacturing process can lead to a continual source of fission product release into the PHTS during steady reactor operation when this contamination is deposited on in-core surfaces.

Such contamination is in the form of fine fuel debris, and therefore the temperature generated by fission heating is generally too low for diffusion to be an important transport process. In this case, direct recoil becomes the dominant release mechanism where the release rate R_{rec} (atom s^{-1}) for the given isotopes of interest from a small particle deposited on an underlying surface is given by [4,10]

$$R_{rec} = \frac{1}{2} F_t y, \tag{10}$$

where y is the fission yield. The tramp uranium fission rate, F_t, can be estimated from a coolant-activity analysis of the short-lived radioiodine species based on the methodology detailed in Ref. [4].

2.3.2.2. Production of ^{99}Mo by activation. The alloys used in the plant piping systems and components (i.e., end fittings, feeder and pressure tubes) are subject to corrosion by the reactor coolant. Some of these corrosion products may be transported in-core where they can become activated by the neutron flux. For instance, this results in the production of such radionuclides as ^{60}Co and ^{99}Mo due to activation of the corrosion products, ^{59}Co and ^{98}Mo.

As considered in the RADSOURCE Code, the production rate of ^{99}Mo by activation can be estimated from the measured activity of ^{60}Co in the PHTS ($A^{60}_{c,meas}$ (Bq)) [2]:

$$R^{Mo-99}_{act} = r\left(\frac{\sigma^{98}}{\sigma^{59}}\right)\left(\frac{\lambda^{60}+\beta^{Co}}{\lambda^{60}}\right)A^{60}_{c,meas}, \tag{11}$$

where σ^{98} is the microscopic thermal absorption cross-section for ^{98}Mo (=130 mb at 0.0253 eV), σ^{59} is the microscopic thermal absorption cross-section for ^{59}Co (=37.18b at 0.0253 eV), λ^{60} is the radioactive decay constant for ^{60}Co and β^{Co} is the coolant purification rate constant for Co removal. The ratio r of the number of atoms of ^{98}Mo/^{59}Co can be estimated from the bulk material composition in the pressure tube (i.e., Mo/Co = 25 ppm/10 ppm) and end-fitting body (Stainless Steel 403) (i.e., Mo/Co = 500 ppm/90 ppm). Thus, accounting for an isotopic abundance of 24.1% for ^{98}Mo, $r \sim 1$.

2.3.2.3. Coolant activity mass balance. The mass balance for ^{99}Mo and ^{99}Tc in the coolant during steady reactor operation (i.e., assuming steady-state conditions for the short-lived ^{99m}Tc) is therefore given by

$$\frac{dN^{Mo-99}_c}{dt} = R^{Mo-99} - (\lambda^{Mo-99}+\beta^{Mo})N^{Mo-99}_c, \tag{12a}$$

$$\frac{dN^{Tc-99}_c}{dt} = R^{Tc-99} + \lambda^{Mo-99}N^{Mo-99}_c - \beta^{Tc}N^{Tc-99}_c, \tag{12b}$$

where the following source release rates (i.e., for recoil and activation processes) are defined via Eqs. (10) and (11):

$$R^{Mo-99} = \frac{1}{2}F_t y^{Mo-99} + R^{Mo-99}_{act}, \tag{13a}$$

$$R^{Tc-99} = \frac{1}{2}F_t(y^{d,Tc-99m} + y^{d,Tc-99}) \tag{13b}$$

and y^d is the direct yield, y is the cumulative yield and β is the coolant purification constant. The coolant activities for ^{99}Mo and ^{99}Tc follow on solution of Eq. (12)

$$A^{Mo-99}_c(t) = A^{Mo-99}_{co}e^{-(\lambda^{Mo-99}+\beta^{Mo})t} + \left(\frac{\lambda^{Mo-99}}{\lambda^{Mo-99}+\beta^{Mo}}\right)R^{Mo-99}\left[1-e^{-(\lambda^{Mo-99}+\beta^{Mo})t}\right] \tag{14}$$

and

$$A_{\mathrm{c}}^{\mathrm{Tc-99}}(t) = A_{\mathrm{co}}^{\mathrm{Tc-99}}\mathrm{e}^{-\beta^{\mathrm{Tc}}t} + \left\{R^{\mathrm{Tc-99}} + \left(\frac{\lambda^{\mathrm{Mo-99}}}{\lambda^{\mathrm{Mo-99}}+\beta^{\mathrm{Mo}}}\right)R^{\mathrm{Mo-99}}\right\}\left(\frac{\lambda^{\mathrm{Tc-99}}}{\beta^{\mathrm{Tc}}}\right)[1-\mathrm{e}^{-\beta^{\mathrm{Tc}}t}] + \left\{A_{\mathrm{co}}^{\mathrm{Mo-99}} - \left(\frac{\lambda^{\mathrm{Mo-99}}}{\lambda^{\mathrm{Mo-99}}+\beta^{\mathrm{Mo}}}\right)R^{\mathrm{Mo-99}}\right\}\left(\frac{\lambda^{\mathrm{Tc-99}}}{\lambda^{\mathrm{Mo-99}}+\beta^{\mathrm{Mo}}-\beta^{\mathrm{Tc}}}\right)\left[\mathrm{e}^{-\left(\lambda^{\mathrm{Mo-99}}+\beta^{\mathrm{Mo}}\right)t} - \mathrm{e}^{-\beta^{\mathrm{Tc}}t}\right]. \quad (15)$$

Here, $A_{\mathrm{co}}^{\mathrm{Mo-99}}$ and $A_{\mathrm{co}}^{\mathrm{Tc-99}}$ are the initial activities of ^{99}Mo and ^{99}Tc at the start of the irradiation period.

Finally, the coolant activities of ^{99}Mo and ^{99}Tc after shutdown (S/D) are given by

$$A_{S/D}^{\mathrm{Mo-99}}(t) = A_{\mathrm{o}}^{\mathrm{Mo-99}}\mathrm{e}^{-\left(\lambda^{\mathrm{Mo-99}}+\beta_{S/D}^{\mathrm{Mo}}\right)t} \quad (16)$$

and

$$A_{S/D}^{\mathrm{Tc-99}}(t) = A_{\mathrm{o}}^{\mathrm{Tc-99}}\mathrm{e}^{-\left(\lambda^{\mathrm{Tc-99}}+\beta_{S/D}^{\mathrm{Tc}}\right)t} + (1-f^{\mathrm{Mo-99}})A_{\mathrm{o}}^{\mathrm{Mo-99}}\left(\frac{\lambda^{\mathrm{Tc-99}}}{(\lambda^{\mathrm{Mo-99}}-\lambda^{\mathrm{Tc-99}})+(\beta_{S/D}^{\mathrm{Mo}}-\beta_{S/D}^{\mathrm{Tc}})}\right) \times \left[\mathrm{e}^{-\left(\lambda^{\mathrm{Tc-99}}+\beta_{S/D}^{\mathrm{Tc}}\right)t} - \mathrm{e}^{-\left(\lambda^{\mathrm{Mo-99}}+\beta_{S/D}^{\mathrm{Mo}}\right)t}\right] + A_{\mathrm{o}}^{\mathrm{Tc-99}m}\left(\frac{\lambda^{\mathrm{Tc-99}}}{\lambda^{\mathrm{Tc-99}m}-\lambda^{\mathrm{Tc-99}}}\right)\left[\mathrm{e}^{-\left(\lambda^{\mathrm{Tc-99}}+\beta_{S/D}^{\mathrm{Tc}}\right)t} - \mathrm{e}^{-\left(\lambda^{\mathrm{Tc-99}m}+\beta_{S/D}^{\mathrm{Tc}}\right)t}\right] + \left(\frac{\lambda^{\mathrm{Tc-99}m}f^{\mathrm{Mo-99}}A_{\mathrm{o}}^{\mathrm{Mo-99}}}{(\lambda^{\mathrm{Mo-99}}-\lambda^{\mathrm{Tc-99}m})+(\beta_{S/D}^{\mathrm{Mo}}-\beta_{S/D}^{\mathrm{Tc}})}\right)\left\{\left(\frac{\lambda^{\mathrm{Tc-99}}}{\lambda^{\mathrm{Tc-99}m}-\lambda^{\mathrm{Tc-99}}}\right)\left[\mathrm{e}^{-\left(\lambda^{\mathrm{Tc-99}}+\beta_{S/D}^{\mathrm{Tc}}\right)t} - \mathrm{e}^{-\left(\lambda^{\mathrm{Tc-99}m}+\beta_{S/D}^{\mathrm{Tc}}\right)t}\right] + \left(\frac{\lambda^{\mathrm{Tc-99}}}{(\lambda^{\mathrm{Mo-99}}-\lambda^{\mathrm{Tc-99}})+(\beta_{S/D}^{\mathrm{Mo}}-\beta_{S/D}^{\mathrm{Tc}})}\right)\left[\mathrm{e}^{-\left(\lambda^{\mathrm{Mo-99}}+\beta_{S/D}^{\mathrm{Mo}}\right)t} - \mathrm{e}^{-\left(\lambda^{\mathrm{Tc-99}}+\beta_{S/D}^{\mathrm{Tc}}\right)t}\right]\right\}. \quad (17)$$

Here the term $A_{\mathrm{o}}^{\mathrm{Mo-99}} = A_{\mathrm{co}}^{\mathrm{Mo-99}} + A_{\mathrm{go}}^{\mathrm{Mo-99}}$ accounts for both the steady-state and shutdown (i.e.., washout) source of ^{99}Mo, and

$$A_{\mathrm{o}}^{\mathrm{Tc-99}m} = \left(\frac{\lambda^{\mathrm{Tc-99}m}}{\lambda^{\mathrm{Tc-99}m}+\beta^{\mathrm{Tc}}}\right) \times \left[\frac{1}{2}F_t y^{d,\mathrm{Tc-99}m} + f^{\mathrm{Mo-99}}R^{\mathrm{Mo-99}}\left(\frac{\lambda^{\mathrm{Mo-99}}}{\lambda^{\mathrm{Mo-99}}+\beta^{\mathrm{Mo}}}\right)\right], \quad (18)$$

where $f^{\mathrm{Mo-99}} = 0.88$ is the branching fraction from ^{99}Mo to $^{99\mathrm{m}}$Tc. For an operating period of duration $t = t^*$, $A_{\mathrm{co}}^{\mathrm{Mo-99}} = A_{\mathrm{c}}^{\mathrm{Mo-99}}(t = t^*)$, $A_{\mathrm{go}}{}^{\mathrm{Mo-99}} = R_{\mathrm{dif}}$ and $A_{\mathrm{o}}^{\mathrm{Tc-99}} = A_{\mathrm{c}}^{\mathrm{Tc-99}}(t = t^*)$, i.e., as evaluated from Eqs. (14), (5) and (15), respectively.

3. Discussion

3.1. Example calculation

Based on a coolant activity analysis in Ref. [4] of the short-lived iodine isotopes observed in the Darlington Nuclear Generating Station (DNGS), the corresponding coolant activity behaviour for technetium can be estimated using the model parameters derived in this analysis. In particular, this previous analysis indicates that there is a single defective rod operating at 40 kW/m ($F_f = 6.0\times10^{14}$ fission s^{-1}), with a tramp uranium fission rate of $F_t = 3.6\times10^{12}$ fission s^{-1} [4]. Thus, the coolant activity concentrations of ^{99}Mo and ^{99}Tc can be predicted as a function of time with Eqs. (14)–(17) for a steady period of reactor operation of $t \sim 200$ d followed by a reactor shutdown. This calculation assumes that the coolant activities of ^{99}Mo and ^{99}Tc are initially zero. The average value of the measured ^{60}Co coolant activities in the DNGS (i.e., 0.12 μCi kg^{-1}) can be further used to estimate the ^{99}Mo production by activation. The empirical diffusion coefficient for Mo can be taken equal to that obtained for the iodine analysis in Ref. 4, where $D'_{\mathrm{Mo}} = D'_I = 4.0\times10^{-10}$ s^{-1}. The purification constant $\beta = \varepsilon f/M_{\mathrm{PHTS}}$ where ε is the purification efficiency for the ion-exchange columns for a given species, f is the purification mass flow rate (kg/s) and M_{PHTS} is the mass of the primary heat transport system (kg). Unfortunately, no data exist on the ion-exchange efficiencies (ε) for Mo, Tc and Co which have different ion charges and radii from that of I. For instance, these species have principal oxidation numbers of Mo (4+, 6+), Tc (7+), Co (2+, 3+) and I (1−), with ionic radii of, respectively: 70, 98, 72 and 216 pm. However, from a waste characterization perspective, one can conservatively assume a ~100% efficiency (i.e., similar to that of iodine)

which will maximize the activity on the ion-exchange columns such that $\beta^{Co} = \beta^{Mo} = \beta^{Tc} = \beta^{I} \sim 4 \times 10^{-5}\,s^{-1}$. An experimental investigation is needed to determine the specific efficiencies. These latter coefficients are further assumed, in this example calculation, to be the same for both steady reactor operation and shutdown (so that $\beta = \beta_{S/D}$).

Moreover, from a waste characterization perspective, it is also useful to compare these concentrations against those for the easy-to-measure radionuclide, ^{137}Cs. For instance, the corresponding activity that develops in the coolant during a constant operating period for ^{137}Cs can be evaluated from [4]

$$A_c(t) = \mu F_f y \left\{ \frac{1 - e^{-\phi\tau}}{\phi} + \left(\frac{e^{-\psi\tau} - e^{-\phi\tau}}{(\psi - \phi)} \right) \frac{3}{\psi} [1 - \sqrt{\psi} \cot \sqrt{\psi}] + 6\psi \sum_{n=1}^{\infty} \left(\frac{e^{-\phi\tau} - e^{-n^2\pi^2\tau}}{n^2\pi^2(n^2\pi^2 - \psi)(n^2\pi^2 - \phi)} \right) \right\} + \lambda y \left(\frac{1 - e^{-\phi\tau}}{\beta} \right) \left(\frac{1}{2} F_t \right), \tag{19}$$

where $\psi = \nu/D'$, $\phi = \beta/D'$ and $\tau = D't$. Since both molybdenum and cesium also exhibit a spiking behaviour during reactor shutdown, the cesium spike release can similarly be evaluated from Eq. (9). Here the initial coolant activity at the time of shutdown, which is present from the previous period of operation at time t^*, can be evaluated from Eq. (19) as $A_{co}^{Cs-137} = A_c^{Cs-137}(t = t^*)$. The stored gap activity of ^{137}Cs that develops during irradiation is:

$$A_{go}^{Cs-137} = \left[\frac{(1 - e^{-\psi\tau})}{\psi} - 6 \sum_{n=1}^{\infty} \frac{e^{-\psi\tau} - e^{-n^2\pi^2\tau}}{n^2\pi^2(n^2\pi^2 - \psi)} \right] \mu F_f y. \tag{20}$$

Thus, the steady state and shutdown activities for ^{137}Cs can be calculated from Eqs. (19), (20) and (9) where $D'_{Cs} = 4.0 \times 10^{-10}\,s^{-1}$, $\nu_{Cs} = 1.32\ 10^{-7}\,s^{-1}$ and $\beta^{Cs} = 4 \times 10^{-6}\,s^{-1}$ [4].

The results of this analysis are shown in Fig. 9(a). Since no isotopes of ^{99}Mo and ^{99}Tc are released from defective fuel during steady reactor operation (i.e., while steam is present in the gap) as discussed in Section 2.3, the contributions from these isotopes to the coolant activity in Fig. 9(a) correspond to that for tramp uranium only. The ^{99}Mo is also produced by activation of the corrosion product ^{98}Mo. Hence, these results also apply to the situation when no defective fuel is present. As further shown in Fig. 9(a), all coolant activity contributions that do not result from defective fuel quickly reach an equilibrium state for the given purification constant. On the other hand, there is a continual buildup of the total coolant activity of ^{137}Cs. This continuous activity increase is due to release from the defective rod where there is an on-going production of cesium in the fuel matrix, which diffuses into the fuel-to-clad gap and eventually into the coolant through the breached site. This contribution is in addition to that released from the tramp uranium. On shutdown, as shown in Fig. 9(b), the activity that has been stored in the (steam-filled) gap during steady operations is quickly washed out of the defective rod, resulting in a spike of activity for both ^{137}Cs and ^{99}Mo. Consequently, the coolant activity of the daughter radionuclide ^{99}Tc increases as a result of the decay of the Mo activity spike.

3.2. Predicted scaling ratio for ^{99}Tc/^{137}Cs

The radionuclide activities will accumulate on the ion-exchange (I-X) columns with continuous coolant cleanup during steady reactor operations and following reactor shutdown. Thus, one can integrate over the corresponding curves in Fig. 9(a). Hence, the scaling ratio for ^{99}Tc/^{137}Cs is 5.8×10^{-6}, which is based on the accumulated isotopic activities on the I-X columns over 200 d of steady operation. On the other hand, if defective fuel had not been present, the accumulated activity for ^{137}Cs in the above expression would have only been 0.0411 μCi/kg (i.e., instead of 1.35 μCi/kg), reflecting the tramp uranium contribution. In this case, the scaling ratio would increase by about a factor of 30 yielding a value of 1.9×10^{-4}. In fact, a single sample from the PHTS resins at the DNGS yielded a measured activity ratio for ^{99}Tc/^{137}Cs of 2×10^{-4}.

The previous analysis only considered the calculation of a scaling ratio that would arise during steady operation and neglected the effect of any augmented release due to washout on shutdown. Thus, as follows from Fig. 9(b), a ratio of 3.5×10^{-6} is obtained which is similar to that previously determined for steady operations (i.e., 5.8×10^{-6}). This result is to be expected since cesium, as well as the precursor of technetium (i.e., molybdenum), both exhibit a similar spiking behaviour on shutdown. These ratios for the CANDU reactor can now be compared to that observed in pressurized and boiling water reactors (see Section 3.3).

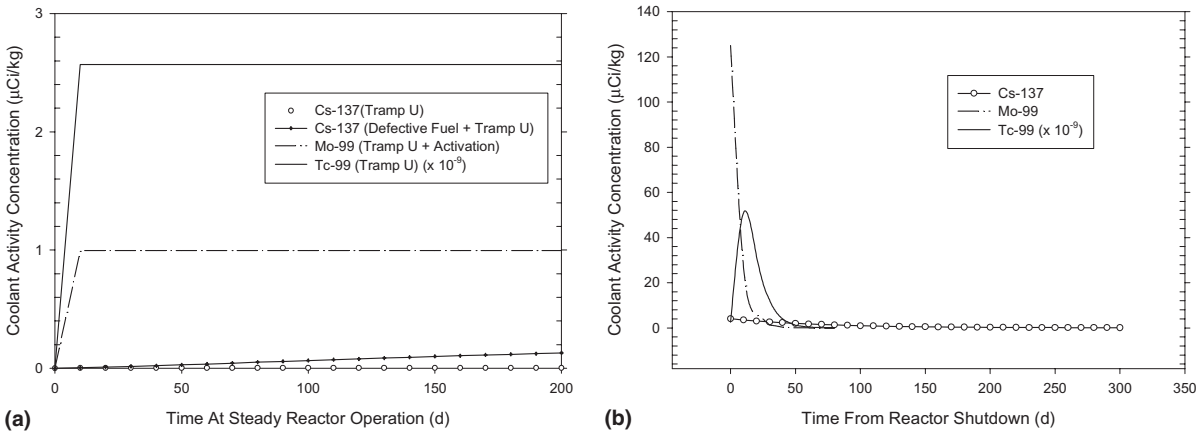

Fig. 9. Coolant activity concentrations of various isotopes for (a) steady reactor operation and (b) for a subsequent reactor shutdown. The initial coolant activity concentrations of ^{137}Cs and ^{99}Mo at the time of shutdown in (b) correspond to the steady state values in (a) plus the spike release contribution.

3.3. Comparison to measured scaling ratios for $^{99}Tc/^{137}Cs$

The Battelle Pacific Northwest Laboratories designed a mixed-bed test resin sampling device to simulate a scaled-down version of the purification demineralizer system for a nuclear power plant [2]. These sampling devices were installed at 10 Pressurized Water Reactors (PWRs) and 7 Boiling Water Reactors (BWRs). The devices were operated with scaled-down flow rates to simulate the cleanup of the reactor coolant (i.e., ~80 ml/min for periods ranging from several days to as long as 6 weeks in the PWR tests and ~42 ml/min for 48 h in the BWR tests). This period of operation is considerably shorter than normal operating times of full-scale purification demineralizer beds (i.e., which are typically employed for up to one year in PWRs). The length of the test resin columns (30 cm) were also relatively short compared to the 90–120 cm deep beds used at PWR stations. The simulated BWR powdered test resins were also operated for considerably less time than actual operations. Radioanalytical techniques were used to measure the concentrations of ^{129}I, ^{99}Tc, ^{90}Sr, ^{238}Pu, ^{239}Pu, ^{240}Pu and ^{14}C. In particular, inductively coupled plasma mass spectrometry (ICPMS), with either a electrothermal vaporization graphite furnace or ultrasonic nebulizer, were used to determine the distributions of ^{99}Tc on the resin columns. Also other gamma emitting radionuclides were measured by gamma spectrometry.

The ^{99}Tc/^{137}Cs ratios can be obtained from the available concentration measurements for the various plant test resin columns [2]. These ratios increase with the number of days sampled in the PWR tests, i.e., the isotopic ratio ranged from 3.5×10^{-9} (0.083 sampling days) to 1.8×10^{-6} (40 sampling days). In comparison, the observed ratio in the BWR tests was several orders of magnitude larger which ranged from 8.5×10^{-6} to 6.6×10^{-3}.

These ratios can be compared to the current analysis performed for the DNGS in Section 3.2, although it is recognized that the activation contribution may differ vastly between different plant designs. Since the Battelle sample devices were installed during steady-state conditions, the steady operation ratio of 5.8×10^{-6} for the DNGS should apply. However, as already mentioned, there is little difference in this ratio with that for shutdown. In fact, the DNGS ratio is within the range of that measured for the PWR and BWR plants. The operation of CANDU reactors would be closer to that of PWRs where no boiling occurs. In fact, the predicted ratio for the DNGS is in reasonable agreement (factor of 3) with that for the PWR Indian Point-2 plant (which had the longest sampling test) [2]. However, it is recognized that the PWR and BWR fuel operate to considerably longer burnups (i.e., ~1000 MWh/kgU versus 180 MWh/kgU) and have much lower heat ratings (20 kW/m versus 40 kW/m). Longer fuel burnups will increase the production of ^{137}Cs in the defective rods but will not influence the amount of ^{99}Mo in the fuel (which will reach equilibrium within ~10 days). Hence, this effect will result in a lower observed ^{99}Tc/^{137}Cs ratio for the light water plants where there is an increased cesium inventory in the coolant but a relatively unchanged amount of technetium (via the decay of the molybdenum that is released from the defective rod). In addition, the effect of deposition of fission products (i.e., Mo and Tc) in the PHTS of the CANDU reactor has been conservatively ignored in the model. The materials are also slightly different in the various reactors, which will affect the activation contribution from the corrosion of ^{98}Mo. BWR plants would presumably experience much greater corrosion rates due

to boiling (and perhaps have a smaller release of water-soluble cesium from defective fuel during steady operation). Hence, these effects would result in much higher scaling ratios for the BWR plants as in fact observed. Thus, the current analysis for the CANDU station appears to be consistent with the observed scaling ratios in the PWR and BWR plants, although it is clear that ^{99}Tc measurements are needed for model validation for the CANDU analysis.

4. Conclusions

1. A model has been developed to estimate the long-lived ^{99}Tc coolant activity as a function time for constant reactor operation and during reactor shutdown. This work considers a thermodynamic treatment using Pourbaix diagrams and a Gibbs-energy minimization to determine the ability for Mo and Tc to leach from defective fuel as well as the chemical form and volatility of these elements. The physical processes of release from the fuel matrix (via a rate-determining step of solid state diffusion to the grain surface and vaporization from this surface into the free spaces) is examined. The production of technetium due to the washout of the parent molybdenum species from defective CANDU fuel rods on reactor shutdown is further modelled. The direct release of technetium from tramp uranium contamination on in-core surfaces is also considered as a continual source of release into the reactor coolant. In addition, the production of technetium from the corrosion and activation of stable molybdenum is estimated in accordance with the measured coolant activity behaviour of ^{60}Co. The resulting activity in the PHTS, and as contained on the ion-exchange columns, is evaluated from mass-balance considerations taking into account the various sources and a loss due to coolant cleanup operations.
2. A coolant activity analysis of the short-lived iodine species and long-lived ^{137}Cs isotope in the DNGS has been used to provide the relevant transport parameters for prediction of the coolant inventories of ^{137}Cs and ^{99}Tc. The sample calculation for this station yields a scaling ratio for ^{99}Tc/^{137}Cs of 6×10^{-6} after ~200 days of steady reactor operation with a single defective fuel rod operating at 40 kW/m. A similar value of 4×10^{-6} is obtained following reactor shutdown with continuous coolant cleanup. This predicted value is consistent with measured coolant activity ratios obtained in test resin samples from pressurized water reactors (4×10^{-9} to 2×10^{-6}) and boiling water reactors (9×10^{-6} to 7×10^{-3}) in a study by the Battelle Pacific Northwest Laboratories. However, ^{99}Tc data for the CANDU reactor are still required for model validation due to inherent differences in the reactor and fuel designs between the light water and CANDU reactors.

Acknowledgments

The current project was identified and managed by Kinectrics Inc., and financially supported by Ontario Power Generation.

References

[1] C. Leuthrot, PROFIP Code Version IV, Commissariat à l'Energie Atomique, Technical Report DEC/SECA/LCC/95-243, 1995.
[2] Vance and Associates, RADSOURCE, Volume 1, Part 1: A Scaling Factor Prediction Computer Technical Manual and Code Validation, Electric Power Research Institute Report, EPRI TR-101969, December 1992.
[3] J. Vance, Topical Report for 3R-STAT: A Tc-99 and I-129 Release Analysis Computer Code, United States Nuclear Regulatory Commission, September 1994.
[4] B.J. Lewis, A. Husain, J. Nucl. Mater. 312 (2003) 81.
[5] M. Pourbaix, Atlas of Electrochemical Equilibria in Aqueous Solutions, Pergamon Press, New York, 1966, p. 209.
[6] E.D. Verink, in: R.W. Revie (Ed.), Uhlig's Corrosion Handbook, Second ed., John Wiley, 2000, p. 111.
[7] C.W. Bale, A.D. Pelton, W.T. Thompson, Centre for Research in Computational Thermodynamics (CRCT), Ecole Polytechnique de Montreal, Montreal, Quebec, 2002.
[8] R. Beraha, G. Beuken, G. Frejaville, C. Leuthrot, Y. Musante, Nucl. Technol. 49 (1980) 426.
[9] B.J. Lewis, C.R. Phillips, M.J. Notley, Nucl. Technol. 73 (1986) 72.
[10] B.J. Lewis, J. Nucl. Mater. 148 (1987) 28.
[11] B.J. Lewis, J. Nucl. Mater. 160 (1988) 201.
[12] C.E. Beyer, EPRI NP-6554, Electric Power Research Institute, September 1989.
[13] D.L. Burman, O.A. Correal, H.W. Wilson, H. Kunishi, L.H. Boman, in: Proc. Int. Top. Mtg. LWR Fuel Performance, Avignon, France, 21–24 April, American Nuclear Society, 1991, p. 363.
[14] B.J. Lewis, R.J. Green, C. Che, Nucl. Technol. 98 (1992) 307.
[15] B.J. Lewis, R.D. MacDonald, N.V. Ivanoff, F.C. Iglesias, Nucl. Technol. 103 (1993) 220.
[16] B.J. Lewis, in: 6th Int. Conf. on CANDU Fuel, ISBN 0-919784-62-3, Niagara Falls, Ontario, 26–29 September 1999, Vol. 1, p. 403.
[17] B.J. Lewis, W.T. Thompson, F. Akbari, D.M. Thompson, C. Thurgood, J. Higgs, J. Nucl. Mater. 328 (2004) 180.
[18] R.J. Lemire, D.J. Jobe, Materials Research Society Symposium Proceedings, Materials Research Society, Vol. 412, 1996, p. 873.
[19] M.H. Kaye, W.T. Thompson, B.J. Lewis, S. Sunder, R. O'Connor, in: 10th International Symposium on

Thermodynamics of Nuclear Materials (STNM-10), Halifax, Nova Scotia, 6–11 August 2000.
[20] M.H. Kaye, W.T. Thompson, B.J. Lewis, S. Sunder, R. O'Connor, in: 7th International Conference on CANDU Fuel, Kingston, Ontario, 23–27 September 2001, p. 3A.
[21] G. Eriksson, W.T. Thompson, CALPHAD 13 (4) (1989) 389.
[22] G. Eriksson, Chem. Scr. 8 (1975) 100.
[23] B.J. Lewis, B.J. Corse, W.T. Thompson, M.H. Kaye, F.C. Iglesias, P. Elder, R. Dickson, Z. Liu, J. Nucl. Mater. 252 (1998) 235.
[24] R.L. Da Silva, D.R. McCracken, K.J. Monserrat, in: I.J. Hastings (Ed.), Advances in Ceramics, Vol. 17, Fission-Product Behaviour in Ceramic Oxide Fuel, American Ceramic Society, Columbus, Ohio, 1986, p. 107.
[25] S. Stroes-Gascoyne, J. Nucl. Mater. 238 (1996) 264.
[26] N.C. Garisto, L.H. Johnson, W.H. Hocking, in: I.J. Hastings (Ed.), Proceedings of the 2nd Int. Conf. on CANDU Fuel, Pembroke, Ontario (Canadian Nuclear Society, Toronto) 1989, p. 352.
[27] S.G. Prussin, D.R. Olander, W.K. Lau, L. Hansson, J. Nucl. Mater. 154 (1988) 25.
[28] I.J. Hastings, Atomic Energy of Canada Limited report AECL-MISC-249, 1982.
[29] H. Kleykamp, J. Nucl. Mater. 84 (1979) 109.
[30] B.M. Jeffery, J. Nucl. Mater. 22 (1967) 33.
[31] B.J. Lewis, B. Andre, G. Ducros, D. Maro, Nucl. Technol. 116 (1996) 34.
[32] R.B. Bird, W.E. Stewart, E.N. Lightfoot, Transport Phenomena, Wiley, New York, 1960.
[33] B.J. Lewis, B. Szpunar, F.C. Iglesias, J. Nucl. Mater. 306 (2002) 30.